Inorganic Chemistry

Article

pubs.acs.org/IC

Novel Fluorite Structured Superparamagnetic $RbGdF_4$ Nanocrystals as Versatile Upconversion Host

Shahzad Ahmad,[†] Rajamani Nagarajan,*[,†] Packiya Raj,[‡] and G. Vijaya Prakash*[,‡]

[†]Materials Chemistry Group, Department of Chemistry, University of Delhi, Delhi 110007, India

[‡]Nanophotonics Laboratory, Department of Physics, Indian Institute of Technology Delhi, New Delhi 110016, India

Supporting Information

ABSTRACT: Fluorite structured nanocrystals of $RbGdF_4$ in cubic symmetry have successfully been synthesized by employing a simple, one-step, and template-free wet chemical method at room temperature. Considering the structural model of cubic $KLaF_4$ in the $Fm\bar{3}m$ space group, the observed powder X-ray diffraction (PXRD) pattern was fitted by the Le Bail procedure with the cubic lattice constant of a = 5.8244 (1) Å. Both high-resolution transmission electron microscopic (HR-TEM) and dynamic light scattering (DLS) measurements revealed the monodispersity of the nanocrystals with their size in the range of 2−18 nm. Upon excitation at 980 nm, Yb^{3+}, (Er^{3+}/Ho^{3+}/Tm^{3+}) codoped $RbGdF_4$ nanocrystals showed multicolor upconversion including red, yellow, blue, and the combination of basic color (near-white) emissions. Also, near-white upconversion emission from Yb^{3+}, Ho^{3+}, Tm^{3+} triply doped cubic $RbGdF_4$ nanocrystals was observed at varying laser power densities. $RbGdF_4$ nanocrystals exhibited superparamagnetic behavior with a molar magnetic susceptibility of 2.61×10^{-2} emu·Oe^{-1}·mol^{-1} at room temperature, while at low temperature (5 K) a saturation magnetization value of 90.41 emu·g^{-1} at an applied field of at 10 kOe was observed. Non-interaction of the localized magnetic moment of Gd^{3+} ions in the host matrix has been reasoned out for the observed superparamagnetic behavior. From the Langevin fit of the magnetic data, the average particle diameter obtained was approximately 2.2 nm, matching well with the values from other measurements. $RbGdF_4$ nanocrystals exhibited a large ionic longitudinal relaxivity (r_1 = 2.30 s^{-1}·mM^{-1}), suggesting their potential applicability as a promising agent for T_1 contrast magnetic resonance imaging (MRI) in addition to the applications arising from the coupling of optical and magnetic functions such as multiplexing biodetection, bioimaging (optical and MRI), and other optical technologies.

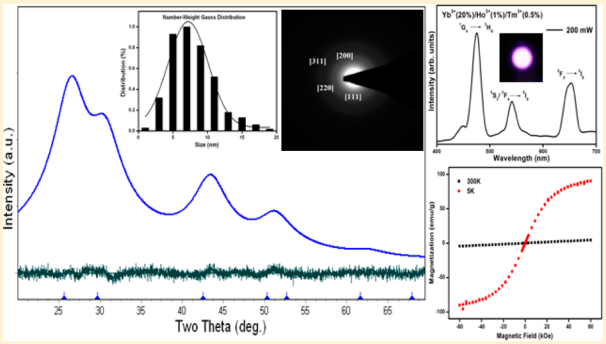

1. INTRODUCTION

Among the f-block elements, gadolinium-containing host matrices are superior as the optical transparency of Gd^{3+} ions in the visible region makes gadolinium ideal for optical applications while having seven of its unpaired inner 4f electrons shielded effectively by the outer electrons $5s^25p^6$ leads to large magnetic moments and long electronic relaxation times suitable for magnetic applications.[1] Furthermore, Gd^{3+}-based mixed metal fluorides as positive contrast agents for magnetic resonance imaging are advantageous over negative contrast agents, such as iron oxide nanoparticles.[2] Earlier, the bifunctionality (of both optical and magnetic) was achieved by doping magnetic Gd^{3+} ions in $NaYF_4$ host matrix in the nanosize regime.[1] By doping Gd^{3+} ions in the $NaYF_4$ nanoparticles, only a portion of the surface of nanoparticles can be covered by Gd^{3+} ions, thus making insufficient availability of these ions for bioapplications such as magnetic resonance imaging (MRI) which are primarily governed by the maximum occupation of Gd^{3+} ions over the surface of these nanoparticles.[1,3,4] Many approaches have been developed to improve the optical and magnetic properties of Gd^{3+} ion containing fluoride host lattices such as varying the crystal phase of the nanoparticles, introducing a codopant as sensitizer, crystal surface coating, and the fabrication of core/shell structures.[5] It is thus desirable to fabricate nanosized Gd^{3+}-containing mixed metal fluorides under controlled reaction conditions. $KGdF_4$ and $NaGdF_4$ are the most widely studied host matrixes known for Gd^{3+}-based mixed metal fluorides. However, the distances between each neighboring Gd^{3+} ion in these host matrixes are not sufficient enough (due to the presence of smaller Na and K ions) to prevent the interaction of localized magnetic moments of Gd^{3+} ions.[6] Moreover, doping of rare earth ions for Gd^{3+} ions brings dopant ions considerably closer, which can lead to deleterious cross-relaxation, resulting in quenching of excitation energy.[7]

Exploring newer host lattices that may influence the radiative and nonradiative transitions involved in the upconversion (UC) process by controlling the local environment such as exchange interaction with the rare earth dopant ions is an important strategy to achieve desirable properties.[8] Recently, Rollet et al.[9] reported the synthesis of $RbLaF_4$ in orthorhombic structure

Received: June 5, 2014
Published: September 25, 2014

(space group *Pnma*), obtained by the solid-state reaction between RbF and LaF_3 at 425 °C under argon atmosphere for 48 h. They showed it to be a good host for luminescence applications. The superiority of a solution based wet chemical process in identifying new phases and metastable polymorphs of thermodynamically stable phases by our research group has motivated the current study to fabricate a fluoride host matrix containing rubidium and gadolinium.[10] It is important to note that the Rb−Gd−F phase diagram has not been investigated in detail and the known compositions, determined from the high temperature solid-state reactions, are $RbGdF_4$ (in hexagonal symmetry), $RbGd_2F_7$ (in orthorhombic symmetry), Rb_3GdF_6 (in cubic symmetry), and $RbGd_3F_{10}$ (in cubic symmetry).[11] It is reported that the decrease in cubic unit-cell volume of the host, caused by the increased size of the alkali metal ion in these systems, can cause an increase in the crystal-field strength around the dopant ions that can potentially lead to enhanced UC efficiency.[7] Thus, $RbGdF_4$ in cubic symmetry would be an ideal host of the all Rb−Gd−F based host matrixes. In addition to its biocompatibility, Rb^+ ions can enhance the Gd−Gd distance within the unit cell, which would improve both optical and magnetic properties.[12] In this paper, the successful synthesis and characterization of new multifunctional fluoride host $RbGdF_4$ nanocrystals in cubic symmetry is described. Use of metal acetylacetonate as a precursor and conducting reactions at room temperature provided efficient control over the phase, morphology, and homogeneity of the products. Additionally, both the optical and magnetic properties of the pure and rare earth ion doped $RbGdF_4$ have been studied.

2. EXPERIMENTAL SECTION

2.1. Synthesis. For the synthesis of $RbGdF_4$, 0.6924 g (4 mmol) of RbF (Sigma-Aldrich; 99.8%) and 0.4542 g (1 mmol) of freshly prepared $Gd(acac)_3$ from Gd_2O_3 (Sigma-Aldrich; 99.9%) were used.[13] The reactants were dissolved independently in 40 mL of methanol. The solution containing the Gd^{3+} ion was added dropwise under constant stirring to RbF solution, and the reaction was continued at room temperature (25 °C) for ∼12 h. A white colored suspension after the reaction was separated by repeated centrifugation at 12 000 rpm and washed with methanol. $YbCl_3$ (Sigma-Aldrich; 99.99%), $HoCl_3$ (Sigma-Aldrich; 99.9%), $TmCl_3$ (Sigma-Aldrich; 99.99%), $ErCl_3$ (Sigma-Aldrich; 99.99%), and $TbCl_3$ (Sigma-Aldrich; 99.9%) were used along with $Gd(acac)_3$ and RbF to synthesize rare earth doped samples following the same procedure employed to make pure $RbGdF_4$.

2.2. Characterization. The powder X-ray diffraction (PXRD) patterns were collected using a PANalytical Empyrean X-ray diffractometer employing Cu Kα radiation (λ = 1.5418 Å) and equipped with a PIXcel^{3D} detector over the range 2θ = 10−70°. High-resolution transmission electron microscopic (HR-TEM) images and energy-dispersive X-ray (EDX) measurements were performed using a Philips Tecnai G^2 30 transmission electron microscope operating at an accelerating voltage of 300 kV. The mean size distribution of nanoparticles was determined by dynamic light scattering (DLS-ZP/Particle Sizer Nicomp 380 ZLS) measurements using the dispersion of nanocrystals in methanol (as solvent). Samples were dispersed using ultrasonic forces, and after dispersion, the pH was measured to be 7.92. Thermogravimetric analysis was carried out using a Mettler Toledo TG/DSC Star^e system at a heating rate of 10 °C/min with the sample mass of ∼6 mg using an alumina pan. The steady-state and time-resolved UC emission measurements in solid form were carried out employing a 980 nm CW laser as the excitation source. The emission light was dispersed into a monochromator (Andor SR-500i-B2) coupled to a CCD detector through an appropriate lens system. For time-resolved emission, a mechanical chopper (12 Hz), a lock-in amplifier, and a monochromator (Acton SP2300) coupled to a photomultiplier tube (PMT) and digital storage oscilloscopes were used. The magnetic measurements were carried out using a vibrating sample magnetometer (Microsense EV9) for room temperature and a superconducting quantum interference device (Ever Cool SQUID VSM DC magnetometer) for variable temperatures. The solvent longitudinal relaxation times (T_1) for the sample dispersed in aqueous solution (H_2O/D_2O = 80/20) were measured using a Bruker Avance NMR spectrometer at 20 °C and at 7.2 T (300 MHz).

3. RESULTS AND DISCUSSION

3.1. Synthesis, Structure, and Morphology. The PXRD pattern of the product from the reaction of RbF with $Gd(acac)_3$ is shown in the Supporting Information, Figure S1. The observed reflections were broad, implying the nanosized nature of crystallites. Reflections in the PXRD pattern were search matched for the known phases of Rb−Gd−F using PANalytical HighScore Plus software, yielding no exact match with the cubic and tetragonal forms of Rb_3GdF_6 (JCPDS Nos. 33-1107 and 27-0522), orthorhombic $RbGd_2F_7$ (JCPDS No. 27-0523), or cubic $RbGd_3F_{10}$ (JCPDS No. 33-1108). In fact, the positions and intensities of the observed reflections in the PXRD pattern closely resembled cubic $KLaF_4$ (JCPDS No. 75-2020) with a slight shift of the reflections to the higher 2θ side. Therefore, cubic $KLaF_4$ (space group $Fm\bar{3}m$ No. 225) was chosen to be the structural model for the simulation of the diffraction peaks using the TOPAS 3 software[14] with the K^+ ion replaced by Rb^+ ions and La^{3+} by Gd^{3+} ions. It is logical that the increment in the ionic size from K^+ (K^{VIII}, 1.65 Å) to Rb^+ (Rb^{VIII}, 1.75 Å) is exactly the same as a reduction in the ionic size from La^{3+} (La^{VIII}, 1.30 Å) to Gd^{3+} (Gd^{VIII}, 1.19 Å), making $RbGdF_4$ in cubic symmetry a natural possibility.[15] The diffractogram was well fit with a lattice constant of a = 5.8244 (1) Å by the Le Bail procedure (Figure 1).[16] The positions of the diffraction peaks

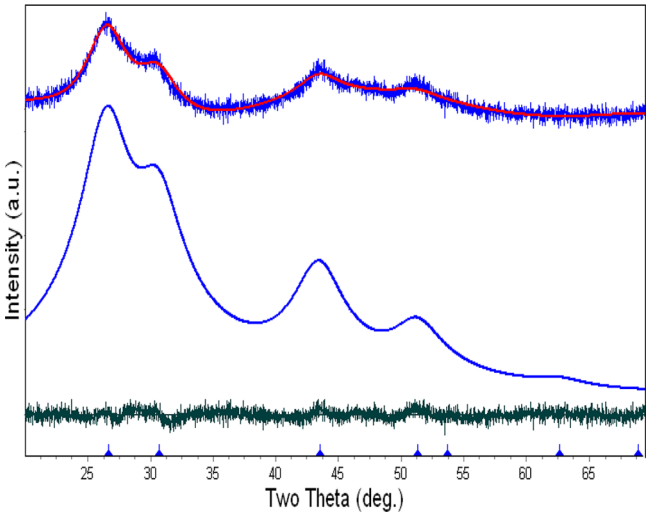

Figure 1. Final Le Bail fit (red line) of the observed PXRD pattern (blue line) of the product from the reaction of RbF with $Gd(acac)_3$ and residuum.

generated considering the fluorite structural model are in good agreement with the measured PXRD pattern. It is therefore concluded that the obtained $RbGdF_4$ possessed fluorite structure. Considering the fluorite structure, the distance between each neighboring Gd^{3+} ion in fluorite structured $RbGdF_4$ is 4.11 Å, a value larger than the values observed in $KGdF_4$ (3.97 Å) and $NaGdF_4$ (3.90 Å). To functionalize

$RbGdF_4$ with optical properties, $Yb^{3+}(20\%)/Er^{3+}(2\%)$, $Yb^{3+}(20\%)/Ho^{3+}(2\%)$, $Yb^{3+}(20\%)/Tm^{3+}(2\%)$, and $Yb^{3+}(20\%)/Ho^{3+}(1\%)/Tm^{3+}(1\%)$ doped $RbGdF_4$ samples were synthesized. PXRD patterns of these samples are shown in Supporting Information, Figure S2, confirming their monophasic nature. Le Bail fitting of the PXRD pattern of $Yb^{3+}(20\%)/Ho^{3+}(1\%)/Tm^{3+}(1\%)$ codoped cubic $RbGdF_4$ sample using GSAS software[17] is shown in Figure 2, which negates the presence of any secondary phase(s).

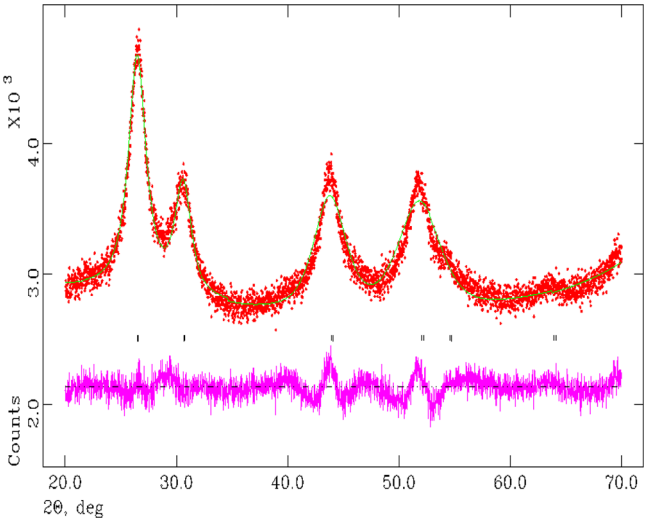

Figure 2. Final Le Bail fit (green line) of the observed PXRD pattern (red line) of $Yb^{3+}(20\%)/Ho^{3+}(1\%)/Tm^{3+}(1\%)$ codoped $RbGdF_4$ sample and residuum.

The morphology, size, and size distribution of $RbGdF_4$ nanocrystals were analyzed by TEM and DLS measurements. In HR-TEM images, the presence of spherical-shaped particles with an average diameter range of about 3−5 nm was evident (Figure 3a). The selected area electron diffraction (SAED) pattern of the crystallites was indexed corresponding to the (111), (200), (220), and (311) planes of cubic $RbGdF_4$ (Figure 3b). The elemental mapping on various locations of the sample was carried out by TEM−EDX analysis (Figure 3c). From the analysis, the concentrations of rubidium, gadolinium, and fluorine were 12.7, 16.3, and 71.0%, respectively, yielding a ratio of 0.8:1.0:4.3. A narrow distribution of particles having diameters in the 2−18 nm range, with an average value of about 7.3 nm, was deduced from the histogram of DLS measurements (Figure 3d). Slow nucleation experiments employing $Gd(acac)_3$ as the precursor for the reactions and conducting the reactions at room temperature are believed to be the reasons for the generation of nanocrystallites with a narrow size distribution. The observed size range has been reported to be quite advantageous for human body clearance, and ideal to display a higher magnetic relaxation.[18]

A TGA trace of $RbGdF_4$ is presented in Supporting Information, Figure S3. $RbGdF_4$ showed thermal stability up to 200 °C. Followed by an initial weight loss (up to 10%) until 200 °C, a further weight loss of 8% occurred between 200 and 600 °C. While the initial mass loss up to 200 °C could be ascribed to the loss of adsorbed moisture (due to high surface energy of the nanocrystallites), the weight loss beyond 200 °C suggested the decomposition of the phase. To verify the nature of the decomposed product, a fresh sample of $RbGdF_4$ was heated at 700 °C for 4 h in a muffle furnace. The PXRD pattern of the resultant solid showed reflections due to orthorhombic RbF (JCPDS No. 78-0661) and tetragonal $Gd_4O_3F_6$ (JCPDS No. 28-0658) as shown in the Supporting Information, Figure S4.

3.2. Upconversion Emission Properties. $RbGdF_4$ nanocrystals functionalized through doping with other rare earth ions (for Gd^{3+}) have been found to exhibit optical properties including the UC emission. Dopant compositions were chosen in such a way that the UC emission occurred in green, yellow, and blue regions. For this, a combination of Yb^{3+} (as sensitizer) with Er^{3+}, Ho^{3+}, and Tm^{3+} ions were doped in $RbGdF_4$. When excited with a 980 nm diode laser, the $Yb^{3+}(20\%)/Er^{3+}(2\%)$, $Yb^{3+}(20\%)/Ho^{3+}(2\%)$, and $Yb^{3+}(20\%)/Tm^{3+}(2\%)$ codoped $RbGdF_4$ nanocrystals exhibited green, yellow, and blue luminescence, respectively, even visible to the naked eye (Figure 4). The weak violet, intense green, and red emissions centered at 410, 522, 545, and 660 nm from the Yb^{3+}/Er^{3+} codoped $RbGdF_4$ sample were attributed to the electronic transitions $^2H_{9/2} \rightarrow {}^4I_{15/2}$, $^2H_{11/2} \rightarrow {}^4I_{15/2}$, $^4S_{3/2} \rightarrow {}^4I_{15/2}$, and $^4F_{9/2} \rightarrow {}^4I_{15/2}$ of Er^{3+} ions, respectively (Figure 4a).[19] Similarly, emission bands centered at 540 and 650 nm, observed for the Yb^{3+}/Ho^{3+} codoped $RbGdF_4$ samples, were associated with the $^5S_2/{}^5F_4 \rightarrow {}^5I_8$ and $^5F_5 \rightarrow {}^5I_8$ transitions of the Ho^{3+} ions, respectively (Figure 4b).[19] For the Yb^{3+}/Tm^{3+} codoped sample, moderate blue (around 477 nm), weak red (around 700 nm), and highly intense near-infrared (800 nm) emissions due to $^1G_4 \rightarrow {}^3H_6$, $^3F_{2,3} \rightarrow {}^3H_6$, and $^3H_4 \rightarrow {}^3H_6$ transitions of Tm^{3+} ions, respectively, resulted (Figure 4c).[19]

The number of photons involved in the UC process, of Yb^{3+}/Er^{3+}, Yb^{3+}/Ho^{3+}, and Yb^{3+}/Tm^{3+} codoped $RbGdF_4$ samples, was determined by studying the pumping power density (P) dependence of the UC emission intensities. In general, the UC emission intensity (I) is expected to be directly proportional to the nth power of the excitation power (P), where n is the number of absorbed photons (>1) for one emitted UC photon. Supporting Information, Figure S5a−c, shows the UC spectra of Yb^{3+}/Er^{3+}, Yb^{3+}/Ho^{3+}, and Yb^{3+}/Tm^{3+} codoped $RbGdF_4$ samples excited with a 980 nm diode laser at various powers. The log−log plots of emission intensity and excitation power are shown in Figure 5a−c, from which slopes of 2.08, 2.10, 1.95, and 1.68 (for the blue, green, and red bands at 410, 522, 545, and 660 nm from the Yb^{3+}/Er^{3+} codoped samples), 1.87 and 2.34 (for the green and red bands at 540 and 650 nm from the Yb^{3+}/Ho^{3+} codoped samples), and 2.36 and 1.80 (for the blue and infrared bands at 475 and 803 nm from the Yb^{3+}/Tm^{3+} codoped samples), respectively, are estimated. These results indicated that the green and red UC emissions only needed two photons, whereas the three-photon process promoted blue UC emission, consistent with previous reports on Y_2O_3, $BaYF_5$, and $NaYF_4$ systems.[20] On the basis of energy-matching conditions, the possible UC mechanisms from the Yb^{3+}/Er^{3+}, Yb^{3+}/Ho^{3+}, and Yb^{3+}/Tm^{3+} codoped $RbGdF_4$ samples are illustrated by a simplified energy level diagram shown in Supporting Information, Figure S6. Figure 5d−f shows the calculated CIE (Commission Internationale de l'Éclairage) color coordinates of the Yb^{3+}/Er^{3+}, Yb^{3+}/Ho^{3+}, and Yb^{3+}/Tm^{3+} codoped $RbGdF_4$ samples for the UC emissions at various powers. When the laser power was changed from 50 to 300 mW, the CIE color coordinates of the UC emission of Yb^{3+}/Er^{3+} codoped $RbGdF_4$ sample shifted only slightly and fell well within the green region (Figure 5d). For the Yb^{3+}/Ho^{3+} codoped $RbGdF_4$ sample, a change of power from 150 to

dx.doi.org/10.1021/ic5013022 | Inorg. Chem. 2014, 53, 10257−10265

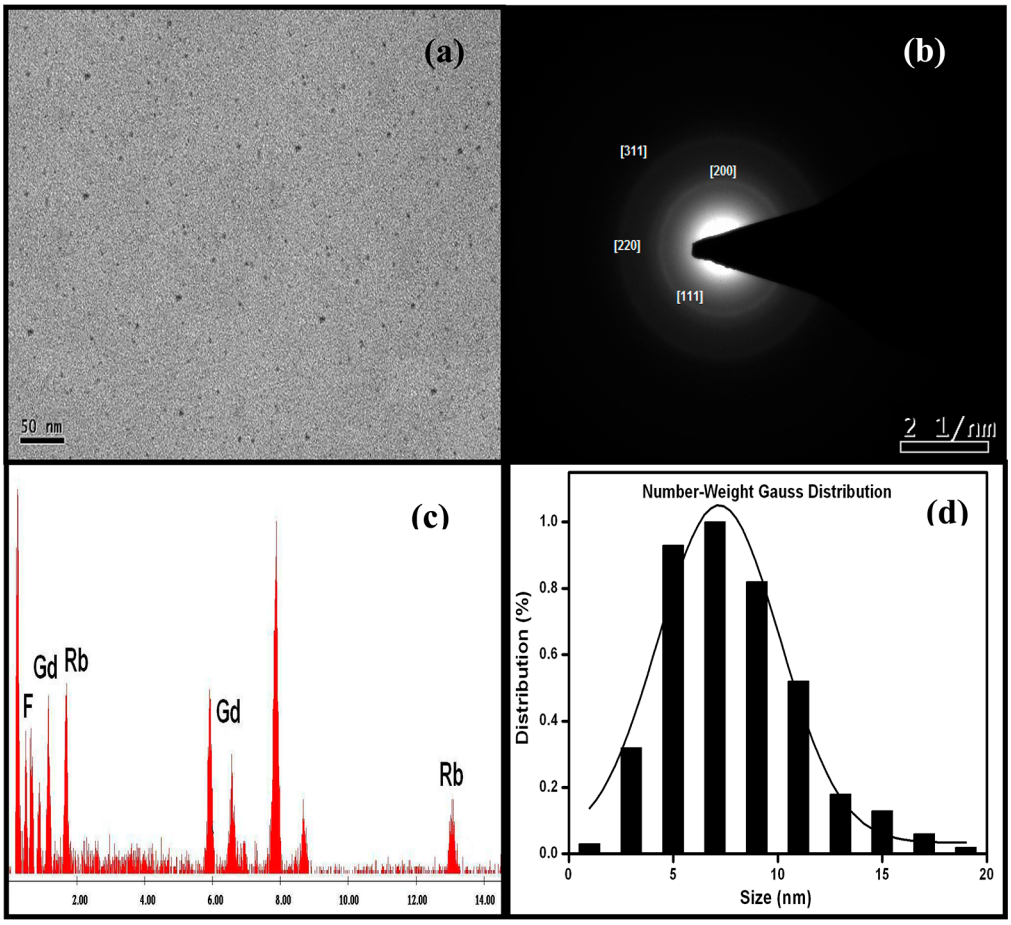

Figure 3. (a) HR-TEM image, (b) SAED pattern, (c) TEM–EDX spectrum, and (d) number-weight Gauss distribution of $RbGdF_4$ nanocrystals (from DLS experiments).

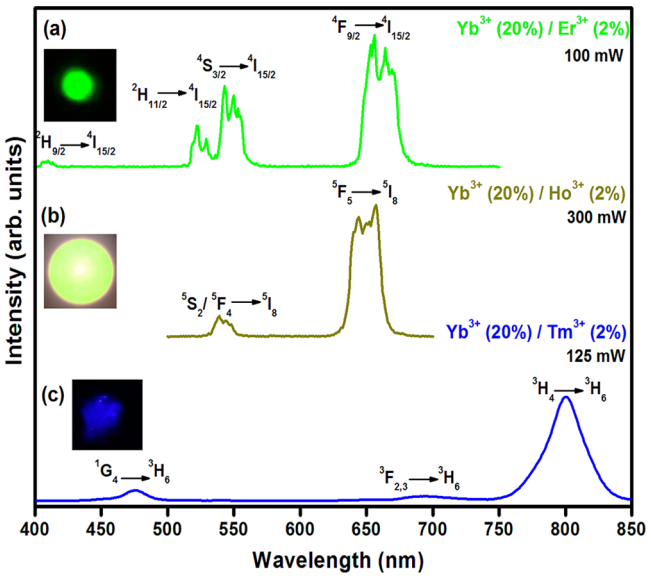

Figure 4. UC emission spectra of (a) Yb^{3+}/Er^{3+}, (b) Yb^{3+}/Ho^{3+}, and (c) Yb^{3+}/Tm^{3+} codoped $RbGdF_4$ samples on excitation with 980 nm diode laser.

450 mW shifted the CIE color coordinates of the UC emission from the greenish yellow to reddish yellow and finally to the bright yellow region, demonstrating that the light outputs could be tuned appropriately by varying the laser power (Figure 5e).

In the case of Yb^{3+}/Tm^{3+} codoped $RbGdF_4$ sample, the CIE color coordinates shifted from whitish blue to the bright blue region in the UC emission when the laser power increased from 25 to 200 mW (Figure 5f). The UC emission lifetimes of Yb^{3+}/Er^{3+}, Yb^{3+}/Ho^{3+}, and Yb^{3+}/Tm^{3+} codoped $RbGdF_4$ samples were calculated from single-exponential fitting ($I = I_0e^{-t/\tau}$, where I_0 is the initial emission intensity and τ is the emission lifetime) of emission decays (Supporting Information, Figure S5d–f). The emission lifetimes for the 545 nm ($^4S_{3/2} \rightarrow {}^4I_{15/2}$ of Er^{3+} ion), 540 and 650 nm ($^5S_2/{}^5F_4 \rightarrow {}^5I_8$ and $^5F_5 \rightarrow {}^5I_8$ of Ho^{3+} ion), and 800 nm ($^3H_4 \rightarrow {}^3H_6$ of Tm^{3+} ion) transitions were 0.245, 0.167, 0.157, and 0.430 ms, respectively. The single-exponential nature of the emission behavior suggested a homogeneous distribution of dopants in the host matrix without any cluster formation.[21]

Nanocrystals showing white UC emission show additional advantages over basic colors UC emission in bioapplications as suggested by recent literature reports.[22] It is quite challenging to achieve white UC emission as its generation requires an adequate combination of the three basic colors (red, green, and blue (RGB)). Usually, a combination of energy level compatible rare earth ions doped in the appropriate host lattice and suitable excitation source have been used to generate white UC emission.[23] White UC emitting $RbGdF_4$ nanocrystals were synthesized by introducing three dopants, viz., Yb^{3+}, Tm^{3+}, and Ho^{3+} ions. As shown in Figure 6a, the white light emission including blue (450 and 475 nm), green (540 nm), and red (640 nm) resulted from $RbGdF_4$:Yb^{3+}(20%)/

dx.doi.org/10.1021/ic5013022 | Inorg. Chem. 2014, 53, 10257–10265

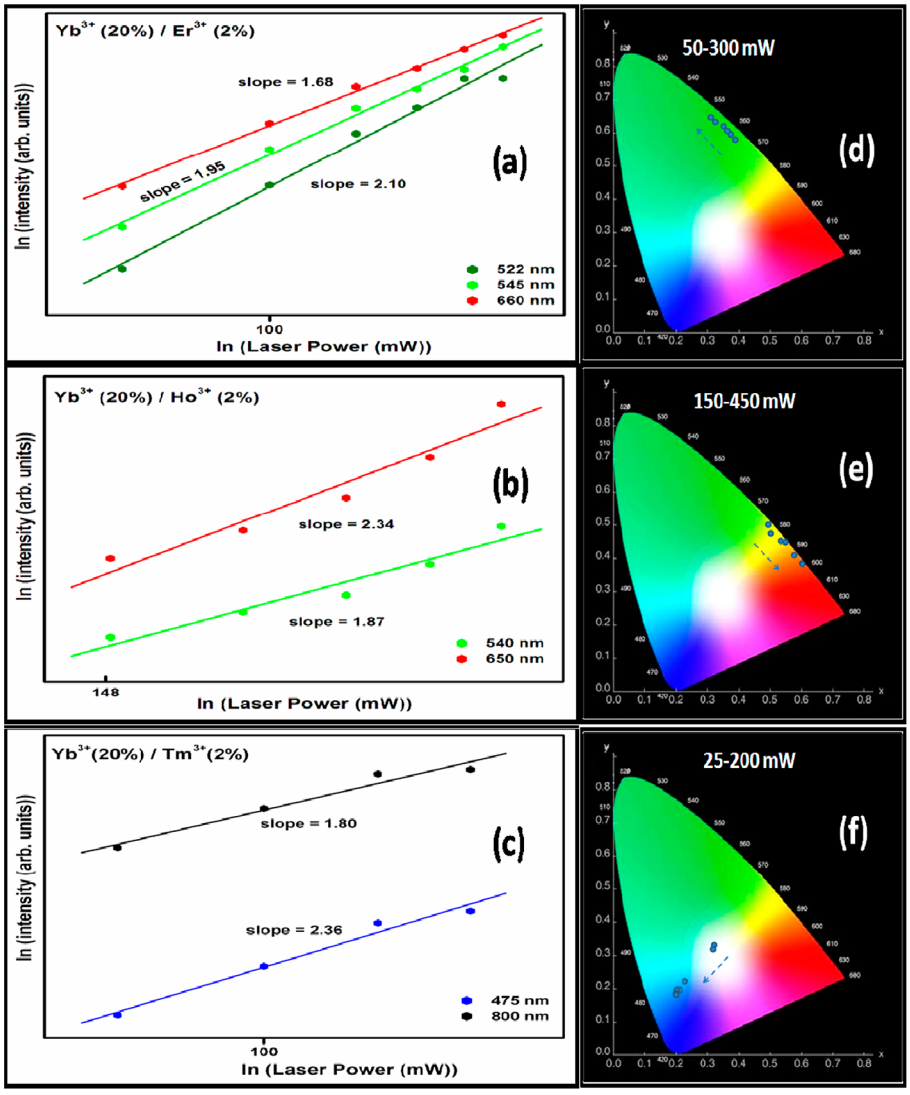

Figure 5. Log–log power dependence of the UC emissions of (a) Yb^{3+}/Er^{3+}, (b) Yb^{3+}/Ho^{3+}, and (c) Yb^{3+}/Tm^{3+} codoped $RbGdF_4$ samples excited with 980 nm diode laser at various powers along with CIE (*X*, *Y*) coordinate diagram showing the chromaticity points calculated from the UC emission spectra of (d) Yb^{3+}/Er^{3+}, (e) Yb^{3+}/Ho^{3+}, and (f) Yb^{3+}/Tm^{3+} codoped $RbGdF_4$ samples.

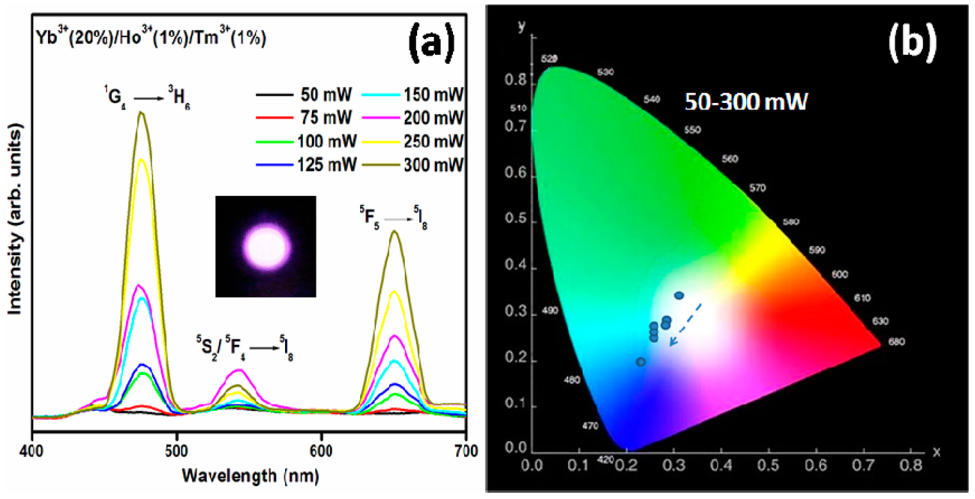

Figure 6. (a) UC emissions of $Yb^{3+}/Ho^{3+}/Tm^{3+}$ codoped $RbGdF_4$ sample excited with 980 nm diode laser at various powers. (b) Corresponding CIE (*X*, *Y*) coordinate diagram showing the chromaticity points.

dx.doi.org/10.1021/ic5013022 | *Inorg. Chem.* 2014, 53, 10257–10265

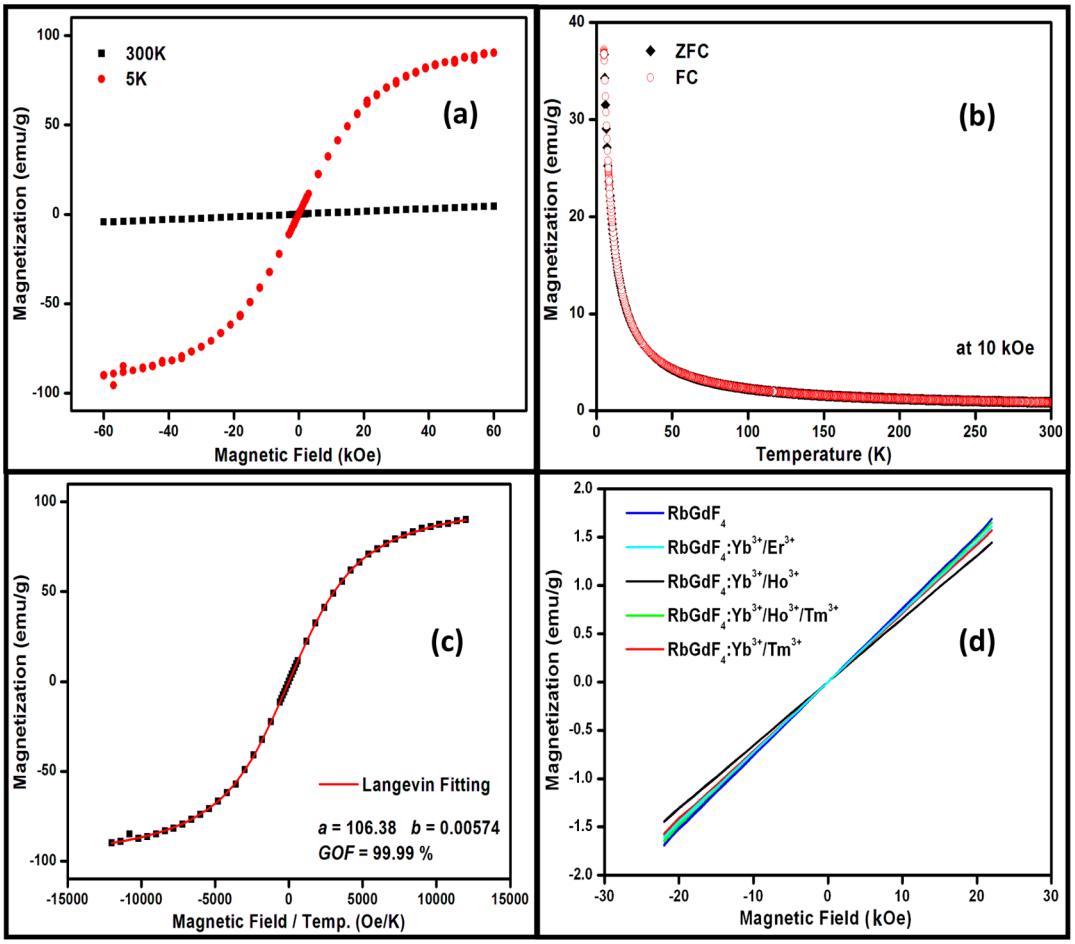

Figure 7. (a) Plot of magnetization as a function of applied field (±60 kOe) at 5 and 300 K. (b) Temperature dependent ZFC−FC magnetization curves of $RbGdF_4$ nanocrystals at an applied field of 10 kOe. (c) Langevin fit for magnetization vs H/T plots. (d) Magnetization plots of undoped and rare earth ion doped $RbGdF_4$ samples as a function of applied field (±22 kOe) at 300 K.

Ho^{3+}(1%)/Tm^{3+}(1%) nanocrystals. In the CIE color coordinates, the position of the UC emission at various laser powers (50−300 mW) fell within the white region (Figure 6b). Moreover, at 50 mW laser power, the calculated chromaticity coordinates were $X = 0.32$, $Y = 0.33$, a value very close to the standard white light ($X = 0.33$, $Y = 0.33$) radiation, suggesting its potential application as a white light source. The logarithmic plots of the emission intensity as a function of excitation power of the blue, green, and red emissions are plotted in the Supporting Information, Figure S7a. The slopes of linear fits for the blue and red bands at 475, 540, and 640 nm from $RbGdF_4$:Yb^{3+}(20%)/Ho^{3+}(1%)/Tm^{3+}(1%) nanocrystals were 2.53, and 2.21, respectively. The emission lifetimes for 475 nm ($^1G_4 \rightarrow {}^3H_6$ of Tm^{3+} ion) and 650 nm ($^5F_5 \rightarrow {}^5I_8$ of Ho^{3+} ion) were 0.277 and 0.245 ms, respectively (Supporting Information, Figure S7b).

3.3. Magnetic Properties. The magnetic measurements of $RbGdF_4$ nanocrystals were carried out using a SQUID magnetometer in magnetic fields up to 60 kOe and temperatures to 5 K. From the field-dependent magnetization plots, superparamagnetic behavior of $RbGdF_4$ nanocrystals was evident with the molar magnetic susceptibility of 2.61×10^{-2} emu·Oe^{-1}·mol^{-1} at room temperature (300 K). This is higher compared to the reported values for $NaGdF_4$ and $KGdF_4$ nanoparticles (Figure 7a). In Table 1, typical molar magnetic susceptibility values available for $NaGdF_4$, $KGdF_4$, and $RbGdF_4$ (of the current study) in nanosizes are listed.[24] It is clearly seen that the molar magnetic susceptibility of $AGdF_4$ increases with the increase in size of the alkali metal ion, making clear the immense influence of Rb^+ ion on the magnetic properties of the $AGdF_4$ system. At low temperatures (5 K), $RbGdF_4$ nanocrystals showed a saturation magnetization value of 90.41 emu·g^{-1} at an applied field of at 10 kOe (Figure 7a).[25] Zero field cooled (ZFC) and field cooled (FC) curves in the temperature range of 5−300 K are presented in Figure 7b. In both, magnetization increased with a decrease in temperature, suggesting the absence of any kind of magnetic coupling between the spins. Both curves were almost superimposed on one another, a feature typical of superparamagnetic behavior, and this feature has gathered additional support from two

Table 1. Comparison of Molar Magnetic Susceptibility Values Reported for $NaGdF_4$ and $KGdF_4$ Systems with the Observed Value for $RbGdF_4$

host lattice	molar magnetic susceptibility (emu·Oe^{-1}·mol^{-1})	ref
$NaGdF_4$	2.02×10^{-2}	25a
	1.62×10^{-2}	25b
	1.68×10^{-2}	25c
$KGdF_4$	2.29×10^{-2}	25d
	2.40×10^{-2}	25e
	2.00×10^{-2}	25f
$RbGdF_4$	2.61×10^{-2}	this work

dx.doi.org/10.1021/ic5013022 | Inorg. Chem. 2014, 53, 10257−10265

points.[26] For noninteracting single domain particles, magnetization as a function of H/T (H = applied magnetic field, T = temperature) can be fitted as per the Langevin equation.[27]

$$M = M_s\left[\coth\left(\frac{\mu_c H}{k_B T}\right) - \frac{1}{\frac{\mu_c H}{k_B T}}\right] \quad (1)$$

where M, M_s, H, and μ_c represent the magnetization, saturation magnetization, applied magnetic field, and magnetic moment of the superparamagnetic compound, respectively, and T denotes temperature. k_B is the Boltzmann constant. For the $RbGdF_4$ nanocrystals, the plot of M/M_s vs H/T at different temperatures converges into one universal curve and can be fitted to the Langevin equation with 99.99% accuracy as shown in Figure 7c. The single-size Langevin model provides a good fit for a whole range of applied magnetic fields, indicating that the particles in our sample are almost of the same size.[27a] The other condition for superparamagnetic behavior is the absence of the hysteresis loop of isothermal magnetization versus applied magnetic field with zero coercivity and remanence.[27b] The superparamagnetic behavior also suggested noninteraction of localized magnetic moments of Gd^{3+} ions, possibly promoted by greater separation between them by the bigger Rb^+ ions. From the Langevin fit, the average particle size of superparamagnetic nanocrystals is estimated using the expression

$$y = a\left[\coth(bx) - \frac{1}{bx}\right] \quad (2)$$

where $x = H/T$, $y = M$, $a = M_s$, and $b = \mu_c/k_B$.

The magnetic moment is

$$\mu_c = M_{sat} V \quad (3)$$

where M_{sat} is the saturation moment of the bulk compound and V is the average particle volume of the superparamagnetic compound.[27c]

As spherical particles were observed for $RbGdF_4$ nanocrystals (in their TEM image, Figure 3), their volume was considered as $V = \pi D^3/6$, where D is the particle diameter.[27d] The theoretical saturation moment of bulk $RbGdF_4$ was calculated to be 138.92 emu·g^{-1} by considering 7.93 unpaired electrons per Gd(III) atom in $RbGdF_4$. From the Langevin fit of the M vs H/T plot (Figure 7c), the parameters a and b were solved to obtain the particle diameter. The average particle diameter obtained by this method was 2.2 nm, matching well with the values found from other techniques. The magnetic moment, calculated from the room temperature magnetic data, was 7.92 μB, matching closely with the spin-only value of 7.93 μB for the Gd^{3+} ion. It is relevant to point out here that the superparamagnetic nanoparticles are essential for applications in biomedicine and biotechnology.[28] Rare earth ion doped $RbGdF_4$ nanocrystals also showed superparamagnetic behavior at an applied field range of ±22 kOe and at room temperature as shown in Figure 7d.

The longitudinal relaxation time (T_1) was measured in aqueous solutions with different concentrations of $RbGdF_4$ nanocrystals. The ionic longitudinal relaxivity (r_1), which is defined as the change in relaxation rate per unit concentration, was obtained for $RbGdF_4$ nanocrystals using the expression[29]

$$1/T_{1(\text{Presence})} = 1/T_{1(\text{Absence})} + r_1[C] \quad (4)$$

where C is the concentration of the $RbGdF_4$ nanocrystals and $T_{1(\text{Presence})}$ and $T_{1(\text{Absence})}$ are the observed longitudinal relaxation times in the presence and absence of $RbGdF_4$ nanocrystals, respectively. From the slope of the plot of $1/T_1$ versus the $RbGdF_4$ concentration (Figure 8), the ionic

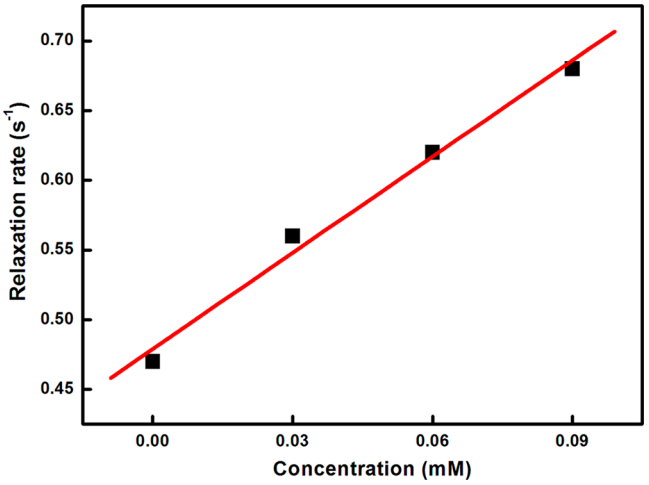

Figure 8. ^{1}H spin−lattice relaxation rates ($1/T_1$) of H_2O as a function of molar concentration of $RbGdF_4$ nanocrystals in 80/20 (v/v) H_2O/D_2O mixture at room temperature and 7.2 T (300 MHz).

longitudinal relaxivity (r_1) was determined to be 2.30 s^{-1}·mM^{-1}. This enhancement of ionic longitudinal relaxivity may be attributed to the smaller size of $RbGdF_4$ nanocrystals with high surface-to-volume ratio, providing more Gd^{3+} ions on the surface and promoting facile magnetic exchange with surrounding water protons.[29] Also, these results demonstrated the potentiality of $RbGdF_4$ nanocrystals as agents for T_1 contrast MRI imaging in addition to the known gadolinium based inorganic nanocrystals.

4. CONCLUSION

In summary, we have demonstrated a simple, template-free, and one-step synthesis of the newer host $RbGdF_4$ in cubic symmetry via a wet chemical method at room temperature. Use of metal acetylacetonate as a precursor played a unique and critical role in controlling the size and morphology of the nanoparticles. HR-TEM and DLS measurements indicated monodispersity of the nanoparticles within the range 2−18 nm. $RbGdF_4$ crystallized in the fluorite structure as confirmed from Le Bail fitting of the PXRD pattern as well as from the SAED pattern. On excitation with a 980 nm laser, the rare earth doped $RbGdF_4$ nanocrystals showed multicolor upconversion emissions, including red, yellow, blue, and white light. Also, white color upconversion emission occurred in $Yb^{3+}/Ho^{3+}/Tm^{3+}$ triply doped $RbGdF_4$ nanocrystals by simply varying the laser power of excitation. $RbGdF_4$ nanocrystals exhibited superparamagnetic behavior and showed large ionic longitudinal relaxivity, indicating their potential applicability as an agent for T_1 contrast MRI imaging. Unlike other multifunctional nanocomposites, $RbGdF_4$:RE^{3+} (RE, rare earth) nanocrystals themselves exhibit multimodality due to the doped rare earth ions contributing to upconversion luminescence with Gd^{3+} ions appending magnetic functions to them. This unique combination might make this system potential multimodal imaging probe work in both optical and magnetic resonance imaging.

dx.doi.org/10.1021/ic5013022 | Inorg. Chem. 2014, 53, 10257−10265

■ ASSOCIATED CONTENT

Supporting Information

PXRD patterns of $RbGdF_4$ and rare earth ion doped $RbGdF_4$, TGA trace of $RbGdF_4$, UC spectra, luminescence decay curves of the rare earth ion doped $RbGdF_4$ samples, and a proposed energy level diagram. This material is available free of charge via the Internet at http://pubs.acs.org.

■ AUTHOR INFORMATION

Corresponding Authors

*E-mail: rnagarajan@chemistry.du.ac.in.

*E-mail: prakash@physics.iitd.ac.in.

Notes

The authors declare no competing financial interest.

■ ACKNOWLEDGMENTS

The authors acknowledge the financial support from DST (SR/S1/PC-08/2012), Government of India, to carry out this work. The authors thank Dr. S. Uma for permitting us to use her DST-funded facilities. The authors thank Prof. Pavan Mathur for useful discussions on magnetic relaxivity measurements. S.A. expresses his sincere thanks to CSIR, New Delhi, India, for the Ex-SRF fellowship. This project is partly supported by the High-Impact Research initiative of IIT Delhi.

■ REFERENCES

(1) (a) Liu, Y.; Tu, D.; Zhu, H.; Li, R.; Luo, W.; Chen, X. *Adv. Mater.* **2010**, *22*, 3266−3271. (b) Kumar, R.; Nyk, M.; Ohulchanskyy, T. Y.; Flask, C. A.; Prasad, P. N. *Adv. Funct. Mater.* **2009**, *19*, 853−859. (c) Park, Y. I.; Kim, J. H.; Lee, K. T.; Jeon, K. S.; Na, H. B.; Yu, J. H.; Kim, H. M.; Lee, N.; Choi, S. H.; Baik, S.-I.; Kim, H.; Park, S. P.; Park, B. J.; Kim, Y. W.; Lee, S. H.; Yoon, S.-Y.; Song, I. C.; Moon, W. K.; Suh, Y. D.; Hyeon, T. *Adv. Mater.* **2009**, *21*, 4467−4471. (d) Abel, K. A.; Boyer, J.-C.; van Veggel, F. C. J. M. *J. Am. Chem. Soc.* **2009**, *131*, 14644−14645.

(2) (a) Dong, C.; Korinek, A.; Blasiak, B.; Tomanek, B.; van Veggel, F. C. J. M. *Chem. Mater.* **2012**, *24*, 1297−1305. (b) Wegh, R. T.; Donker, H.; Oskam, K. D.; Meijerink, A. *Science* **2009**, *283*, 663−666. (c) Liu, C.; Gao, Z.; Zeng, J.; Hou, Y.; Fang, F.; Li, Y.; Qiao, R.; Shen, S.; Lei, H.; Yang, W.; Gao, M. *ACS Nano* **2013**, *7*, 7227−7240. (d) Lee, J.; Lee, T. S.; Ryu, J.; Hong, S.; Kang, M.; Im, K.; Kang, J. H.; Lim, S. M.; Park, S.; Song, R. *J. Nucl. Med.* **2013**, *54*, 96−103.

(3) *Advances in Inorganic Chemistry*; Eldik, R. V., Bertini, I., Eds.; Elsevier Academic Press: Amsterdam, 2005; Vol. *57*.

(4) (a) Ryu, J.; Park, H.-Y.; Kim, K.; Kim, H.; Yoo, J. H.; Kang, M.; Im, K.; Grailhe, R.; Song, R. *J. Phys. Chem. C* **2010**, *114*, 21770−21774. (b) Zhou, J.; Yu, M.; Sun, Y.; Zhang, X.; Zhu, X.; Wu, Z.; Wu, D.; Li, F. *Biomaterials* **2011**, *32*, 1148−1156. (c) Liu, Q.; Sun, Y.; Li, C.; Zhou, J.; Li, C.; Yang, T.; Zhang, X.; Yi, T.; Wu, D.; Li, F. *ACS Nano* **2011**, *5*, 3146−3157. (d) Cheng, L.; Yang, K.; Li, Y.; Chen, J.; Wang, C.; Shao, M.; Lee, S.-T.; Liu, Z. *Angew. Chem., Int. Ed.* **2011**, *50*, 7385−7390. (e) Johnson, N. J. J.; Oakden, W.; Stanisz, G. J.; Prosser, R. S.; van Veggel, F. C. J. M. *Chem. Mater.* **2011**, *23*, 3714−3722.

(5) (a) Wang, F.; Han, Y.; Lim, C. S.; Lu, Y.; Wang, J.; Xu, J.; Chen, H.; Zhang, C.; Hong, M.; Liu, X. *Nature* **2010**, *463*, 1061−1065. (b) Niu, W.; Wu, S.; Zhang, S.; Li, L. *Chem. Commun.* **2010**, *46*, 3908−3910. (c) Chen, D.; Yu, Y.; Huang, F.; Huang, P.; Yang, A.; Wang, Y. *J. Am. Chem. Soc.* **2010**, *132*, 9976−9978. (d) Wang, F.; Wang, J.; Liu, X. *Angew. Chem., Int. Ed.* **2010**, *49*, 7456−7460. (e) Yi, G. S.; Chow, G. M. *Adv. Funct. Mater.* **2006**, *16*, 2324−2329. (f) Li, D.; Dong, B.; Bai, X.; Wang, Y.; Song, H. *J. Phys. Chem. C* **2010**, *114*, 8219−8226. (g) Vetrone, F.; Naccache, R.; Mahalingam, V.; Morgan, C. G.; Capobianco, J. A. *Adv. Funct. Mater.* **2009**, *19*, 2924−2929.

(6) He, F.; Niu, N.; Wang, L.; Xu, J.; Wang, Y.; Yang, G.; Gai, S.; Yang, P. *Dalton Trans.* **2013**, *42*, 10019−10028.

(7) Wang, F.; Liu, X. *Chem. Soc. Rev.* **2009**, *38*, 976−989.

(8) (a) Schaefer, H.; Ptacek, P.; Zerzouf, O.; Haase, M. *Adv. Funct. Mater.* **2008**, *18*, 2913−2918. (b) Chen, D.; Yu, Y.; Huang, F.; Huang, P.; Yang, A.; Wang, Z.; Wang, Y. *Chem. Commun.* **2011**, *47*, 11083−11085.

(9) Rollet, A.-L.; Allix, M.; Veron, E.; Deschamps, M.; Montouillout, V.; Suchomel, M. R.; Suard, E.; Barre, M.; Ocaña, M.; Sadoc, A.; Boucher, F.; Bessada, C.; Massiot, D.; Fayon, F. *Inorg. Chem.* **2012**, *51*, 2272−2282.

(10) (a) Ahmad, S.; Prakash, G. V.; Nagarajan, R. *Inorg. Chem.* **2012**, *51*, 12748−12754. (b) Das, S.; Reddy, A. A.; Ahmad, S.; Nagarajan, R.; Prakash, G. V. *Chem. Phys. Lett.* **2011**, *508*, 117−120. (c) Ahmad, S.; Das, S.; Nagarajan, R.; Prakash, V. G. *Opt. Mater.* **2013**, *36*, 396−401.

(11) (a) Shaimuradov, I. B.; Reshetnikova, L. P.; Novoselova, A. V. *Russ. J. Inorg. Chem.* **1974**, *19*, 1642−1643. (b) Védrine, A.; Boutonnet, R.; Sabatier, R.; Cousseins, J. C. *Bull. Soc. Chim. Fr.* **1975**, *3*−*4*, 445−448. (c) Pistorious, C. W. F. T. *Mater. Res. Bull.* **1974**, *9*, 1337−1344. (d) Hebecker, C.; Losch, R. *Naturwissenschaften* **1975**, *62*, 37−37.

(12) (a) Cesareo, R.; Principe, D. D.; Tallarida, B.; Mancuso, G. *Eur. J. Nucl. Med.* **1978**, *3*, 91−93. (b) Gould, K. L.; Yoshida, K.; Hess, M. J.; Haynie, M.; Mullani, N.; Smalling, R. W. *J. Nucl. Med.* **1991**, *32*, 1−9. (c) Yen, C. K.; Yano, Y.; Budinger, T. F.; Friedland, R. P.; Derenzo, S. E.; Huesman, R. H.; O'Brien, H. A. *J. Nucl. Med.* **1982**, *23*, 532−537. (d) Jadvar, H. Parker, J. A. *Clinical PET and PET/CT*; Springer: New York, 2005. (e) Wagner, F. S. *Kirk-Othmer Encyclopedia of Chemical Technology*; Wiley: Hoboken, NJ, 2011; pp 1−11.

(13) Stites, J. G.; McCarty, C. N.; Quill, L. L. *J. Am. Chem. Soc.* **1948**, *70*, 3142−3143.

(14) Coelho, A. A. *TOPAS User Manual*, version 3.1; Bruker AXS GmbH, Karlsruhe, Germany, 2003.

(15) Shannon, R. D.; Prewitt, C. T. *Acta Crystallogr.* **1970**, *B26*, 1046−1048.

(16) Le Bail, A.; Duroy, H.; Fourquet, J. L. *Mater. Res. Bull.* **1988**, *23*, 447−452.

(17) Larson, A. C.; Von Dreele, R. B. *General Structure Analysis System (GSAS)*; Los Alamos National Laboratory Report, LAUR, 86; Los Alamos National Laboratory: Los Alamos, NM, 1994.

(18) (a) Chen, G.; Ohulchanskyy, T. Y.; Law, W. C.; Argen, H.; Prasad, P. N. *Nanoscale* **2011**, *3*, 2003−2008. (b) Bridot, J.-L.; Faure, A. C.; Laurent, S.; Rivière, C.; Billotey, C.; Hiba, B.; Janier, M.; Josserand, V.; Coll, J.-L.; Elst, L. V.; Muller, R.; Roux, S.; Perriat, P.; Tillement, O. *J. Am. Chem. Soc.* **2007**, *129*, 5076−5084.

(19) Reisfeld, R.; Jorgensen, C. K. *Laser and Excited States of Rare Earths*; Springer-Verlag: Berlin, 1977.

(20) (a) Chen, G.; Liu, Y.; Zhang, Y.; Somesfalean, G.; Zhang, Z.; Sun, Q.; Wang, F. *Appl. Phys. Lett.* **2007**, *91*, 133103. (b) Vetrone, F.; Mahalingam, V.; Capobianco, J. *Chem. Mater.* **2009**, *21*, 1847−1851. (c) Yin, A.; Zhang, Y.; Sun, L.; Yan, C. *Nanoscale* **2010**, *2*, 953−959.

(21) Stouwdam, J. W.; van Veggel, F. C. J. M. *Nano Lett.* **2002**, *2*, 733−737.

(22) (a) Weiss, S. *Science* **1999**, *283*, 1676−1683. (b) Wang, L. Y.; Yan, R. X.; Huo, Z. Y.; Wang, L.; Zeng, J. H.; Bao, J.; Wang, X.; Peng, Q.; Li, Y. D. *Angew. Chem., Int. Ed.* **2005**, *44*, 6054−6057.

(23) (a) Downing, E.; Hesselink, L.; Ralston, J.; Macfarlane, R. *Science* **1996**, *273*, 1185−1189. (b) Chen, D.; Wang, Y.; Zheng, K.; Guo, T.; Yu, Y.; Huang, P. *Appl. Phys. Lett.* **2007**, *91*, 251903. (c) Li, J. J.; Yang, L. W.; Zhang, Y. Y.; Zhong, J. X.; Sun, C. Q.; Chu, P. K. *Opt. Mater.* **2011**, *33*, 882−887.

(24) (a) Li, F.; Li, C.; Liu, X.; Chen, Y.; Bai, T.; Wang, L.; Shi, Z.; Feng, S. *Chem.—Eur. J.* **2012**, *18*, 11641−11646. (b) Ren, G.; Zeng, S.; Hao, J. *J. Phys. Chem. C* **2011**, *115*, 20141−20147. (c) Wang, Z.-L.; Hao, J. H.; Chan, H. L. W. *J. Mater. Chem.* **2010**, *20*, 3178−3185. (d) Ju, Q.; Tu, D.; Liu, Y.; Li, R.; Zhu, H.; Chen, J.; Chen, Z.; Huang, M.; Chen, X. *J. Am. Chem. Soc.* **2012**, *134*, 1323−1330. (e) Yang, D.; Li, G.; Kang, X.; Cheng, Z.; Ma, P.; Peng, C.; Lian, H.; Li, C.; Lin, J. *Nanoscale* **2012**, *4*, 3450−3459. (f) Yang, L. W.; Zhang, Y. Y.; Li, J. J.; Li, Y.; Zhong, J. X.; Chu, P. K. *Nanoscale* **2010**, *2*, 2805−2810.

(25) (a) Jeun, M.; Jeoung, J. W.; Moona, S.; Kim, Y. J.; Lee, S.; Paek, S. H.; Chung, K.-W.; Park, K. H.; Bae, S. *Biomaterials* **2011**, *32*, 387−394. (b) Huang, C.-C.; Liu, T.-Y.; Su, C.-H.; Lo, Y.-W.; Chen, J.-H.;

Yeh, C.-S. *Chem. Mater.* **2008**, *20*, 3840−3848. (c) Yu, S.-Y.; Zhang, H.-J.; Yu, J.-B.; Wang, C.; Sun, L.-N.; Shi, W. D. *Langmuir* **2007**, *23*, 7836−7840. (d) Bharde, A. A.; Parikh, R. Y.; Baidakova, M.; Jouen, S.; Hannoyer, B.; Enoki, T.; Prasad, B. L. V.; Shouche, Y. S.; Ogale, S.; Sastry, M. *Langmuir* **2008**, *24*, 5787−5794. (e) Taboada, E.; Rodríguez, E.; Roig, A.; Oró, J.; Roch, A.; Muller, R. N. *Langmuir* **2007**, *23*, 4583−4588. (f) Tartaj, P.; Serna, C. J. *Chem. Mater.* **2002**, *14*, 4396−4402. (g) Sun, X.; Zheng, C.; Zhang, F.; Li, L.; Yang, Y.; Wu, G.; Guan, N. *J. Phys. Chem. C* **2008**, *112*, 17148−17155.

(26) (a) Guo, F.; Zhang, Q.; Zhang, H.; Zhang, B.; Gu, J. *J. Polym. Res.* **2011**, *18*, 745−751. (b) Gao, G.; Zhang, C.; Zhou, Z.; Zhang, X.; Ma, J.; Li, C.; Jin, W.; Cui, D. *Nanoscale* **2013**, *5*, 351−362. (c) Wang, D.; Ren, L.; Zhou, X.; Wang, X.-Z.; Zhou, J.; Han, Y.; Kang, N. *Nanotechnology* **2012**, *23*, 225705.

(27) (a) Chen, D.-X.; Sanchez, A.; Taboada, E.; Roig, A.; Sun, N.; Gu, H.-C. *J. Appl. Phys.* **2009**, *105*, 083924. (b) Desai, P.; Song, K.; Koza, J.; Pariti, A.; Nath, M. *Chem. Mater.* **2013**, *25*, 1510−1518. (c) Callister, W. D., Jr.; Rethwisch, D. G. *Materials Science and Engineering: An Introduction*; Wiley: Hoboken, NJ, 2007. (d) Drago, R. S. *Physical Method for Chemists*, 2nd ed.; W. B. Saunders: Philadelphia, PA, 1992.

(28) (a) Gao, G.; Huang, P.; Zhang, Y.; Wang, K.; Qin, W.; Cui, D. *CrystEngComm* **2011**, *13*, 1782−1785. (b) Hu, F.; Wei, L.; Zhou, Z.; Ran, Y.; Li, Z.; Gao, M. *Adv. Mater.* **2006**, *18*, 2553−2556. (c) He, M.; Huang, P.; Zhang, C.; Chen, F.; Wang, C.; Ma, J.; He, R.; Cui, D. *Chem. Commun.* **2011**, *47*, 9510−9512.

(29) (a) Ju, Q.; Tu, D.; Liu, Y.; Li, R.; Zhu, H.; Chen, J.; Chen, Z.; Huang, M.; Chen, X. *J. Am. Chem. Soc.* **2012**, *134*, 1323−1330. (b) Johnson, N. J. J.; Oakden, W.; Stanisz, G. J.; Prosser, R. S.; Veggel, F. C. J. M. *Chem. Mater.* **2011**, *23*, 3714−3722. (c) Bridot, J.-L.; Faure, A.-C.; Laurent, S.; Rivière, C.; Billotey, C.; Hiba, B.; Janier, M.; Josserand, V.; Coll, J. L.; Elst, L. V.; Muller, R.; Roux, S.; Perriat, P.; Tillement, O. *J. Am. Chem. Soc.* **2007**, *129*, 5076−5084.